CHINESE JOURNAL OF PHYSICS VOL. 38, NO. 5 OCTOBER 2000

# Gradient-Corrected Density Functional Calculation of Elastic Constants of Fe, Co and Ni in bcc, fcc and hcp Structures

G. Y. Guo and H. H. Wang
*Department of Physics, National Taiwan University,*
*Taipei, Taiwan 106, R.O.C.*

(Received January 13, 2000)

Systematic *ab initio* calculations of lattice constants, elastic constants and magnetic moments of Fe, Co and Ni in bcc, fcc and hcp structures have been carried out, in part to understand the phase stability and magnetic properties of artificial Fe, Co and Ni structures. The calculations are based on the local spin-density functional theory with generalized gradient corrections (GGA) which are found to describe the properties of these materials rather well. In particular, the calculated lattice constants and bulk modulus of the observed structures are in good agreement with experiments. Also, the theoretical elastic constants agree with the measurements within the numerical uncertainties. Interestingly, several energetically metastable structures are found to be elastically unstable. It is predicted that magnetism has a pronounced influence on both the size and sign of some elastic constants, and hence on the structural stabilities. For example, while both nonmagnetic Fe fcc and hcp structures are metastable phases, ferromagnetic Fe fcc and hcp structures are not. These results would help to gain insight into the formation of certain artificial thin films and superlattices.

PACS. 62.20.Dc – Elasticity, elastic constants.
PACS. 71.15.Mb – Density functional theory, local density approximation.
PACS. 75.20.En – Metals and alloys.

## I. Introduction

The recent advent of advanced thin film growth techniques has stimulated enormous interest in making artificial crystalline structures that do not exist in nature [1-3]. These artificial systems would allow one to better understand the growth mechanism and structural phase transition and also to explore novel physical properties distinct from that of the natural crystals. Well-known artificial structures include fcc Fe on Cu [1], bcc Co on GaAs [2] and bcc Ni on Fe [3]. Stimulated by these interesting experiments, we have performed systematic first-principles density functional total energy calculations of Fe, Co and Ni in three common structures, namely, bcc, fcc and hcp, in both ferromagnetic and nonmagnetic states.

The purpose of this work is multiple. Firstly, density functional theory (DFT) with the local density approximation (LDA) [4] has been used for first-principles studies of the physical properties of a variety of materials. It provides an accurate theorectical estimate of static structural properties, phonon spectra, crystal stability, and pressure-induced phase transformations in many solids [5]. However, there were also problems in the LDA. Notably, it predicted a wrong ground state for iron [7, 8] and certain alkali metals [9]. There has been some considerable effort

worldwide in recent years to improve and go beyond the LDA [5]. In particular, the so-called generalized gradient corrections (GGA) to the LDA have been developed by several groups (see, e.g., [10] and references therein). These GGA calculations have been found to considerably improve the LDA results in many cases [11]. For example, the GGA calculations predict a correct ground state structure for iron and also substantially reduce the discrepancy in e.g., lattice constants between the theory and experiments [11]. However, a stringent test of the GGA is to calculate the elastic constants of, e.g., $3d$ magnetic metals. Therefore, we have performed systematic DFT-LDA-GGA calculations of elastic constants of Fe, Co and Ni in their observed structures.

Secondly, the density functional total energy of Fe, Co and Ni in a number of structures has been calculated by several groups in the past (e.g., [12]). There is always a minimum in the total energy vs volume curve for every structure considered [12]. However, this does not necessarily mean that these phases are a stable or metastable structure. They could be unstable if at least one of their elastic constants is negative. A good example of elastic instability is bcc Co [13]. Clearly, to better understand the phase stability of the artificial structures, one needs to know the elastic constants of these structures. We thus have calculated the elastic constants of Fe, Co and Ni in their most common bcc, fcc and hcp structures. Note that almost all transition metal artificial magnetic thin films and superlattices contain at least one of these three elements.

Thirdly, since the GGA calculations describe satisfactorily lattice and elastic constants of Fe, Co and Ni in their observed structures, as will be shown below, the GGA predictions for the structural properties of the hithoto unobserved structures are expected to be rather reliable. Therefore, one may be able to use the calculated lattice constants and the signs of calculated elastic constants to help fabricate new artificial structures.

The organization of the rest of this paper is as follows. In the next section, we describe briefly the relevant elastic theory and the determination of the elastic constants of cubic and hexagonal systems via first-principles total energy calculations. Also the computational details will be given. In Sec. III, we present the calculated total energies, lattice constants and bulk modulii. In Sec. IV, we report the calculated elastic constants. In Sec. V, we will discuss the effects of magnetism on the phase stability of Fe, Co and Ni. A short summary is also given in this section.

## II. Elastic theory and computational details

For small strains ($\underline{\epsilon}$) on a solid, the Hook's law is applicable and the elastic energy $E_e$ is approximately a quadratic function of the strain components

$$E_e(V_0, \underline{\epsilon}) = V_0 \sum_{i,j=1}^{6} \frac{1}{2} C_{ij} e_i e_j \tag{1}$$

where $C_{ij}$ are the elastic constants, $V_0$ is the total volume and $e_i$ are the components of the strain tensor

$$\underline{\epsilon} = \begin{pmatrix} e_1 & e_6 & e_5 \\ e_6 & e_2 & e_4 \\ e_5 & e_4 & e_3 \end{pmatrix} \tag{2}$$

in conventional elastic theory notation [14]. Under these strains, the original lattice vectors $\mathbf{a}$ would be transformed into the strained ones $\mathbf{a}'$ as $\mathbf{a}' = (I + \underline{\epsilon})\mathbf{a}$ where $I$ is the identity matrix.

For a cubic crystal, there are only three independent elastic constants, namely, $C_{11}, C_{12}$ and $C_{44}$. Furthermore, the bulk modulus $B$ and tetragonal shear constant $C'$ are related to $C_{11}$ and $C_{12}$, i.e., $B = \frac{1}{3}(C_{11} + 2C_{12})$, $C' = \frac{1}{2}(C_{11} - C_{12})$. $C_{44}$ is the trigonal shear constant. $B = V\frac{d^2E}{dV^2}$ can be determined by fitting the calculated total energy $E$ as a function of volume $V$ to the equation of state of Murnaghan [15]. $C'$ ($C_{44}$) may be determined by a polynormial fiting of the calculated total energy $E$ as a function of the tetragonal (orthorhombic) strain

$$\underline{\epsilon} = \begin{pmatrix} \varepsilon & 0 & 0 \\ 0 & \varepsilon & 0 \\ 0 & 0 & -\frac{\varepsilon(2+\varepsilon)}{(1+\varepsilon)^2} \end{pmatrix} \left(\underline{\epsilon} = \begin{pmatrix} 0 & \varepsilon & 0 \\ \varepsilon & 0 & 0 \\ 0 & 0 & \frac{\varepsilon^2}{1+\varepsilon^2} \end{pmatrix}\right). \tag{3}$$

The associated energy change due to the strain is approximately given by

$$\Delta E(V_0) = \frac{3}{2V_0} C'\varepsilon^2 (\Delta E(V_0) = 2V_0 C_{44}\varepsilon^2). \tag{4}$$

For a hexagonal solid, there are five independent elastic constants, namely, $C_{11}, C_{12}, C_{13}, C_{33}$ and $C_{55}$. Total energy calculation of the elastic constants of a hcp solid is rather involved. Indeed, the elastic constants of only a few elemental hcp metals have been calculated [16]. The five elastic constants of a hcp solid are related to the bulk modulus ($B$) and four shear constants ($C_{11} + C_{12}$, $C_{11} - C_{12}$, $\frac{1}{2}C_{33}$ and $2C_{55}$) [16]. The $B$ can be written as

$$B = \frac{2}{9}\left(C_{11} + C_{12} + 2C_{13} + \frac{1}{2}C_{33}\right). \tag{5}$$

Here, we determine the four shear constants (hence the elastic constants) by a polynormial fitting of the calculated total energy as a function of the shear strains, as described in Ref [16]. The shear constants ($C_{11} + C_{12}$) and $C_{33}$ correspond to the uniform in-plane strain and the interlayer strain with the strain matrice

$$\begin{pmatrix} \varepsilon & 0 & 0 \\ 0 & \varepsilon & 0 \\ 0 & 0 & 0 \end{pmatrix} \tag{6}$$

and

$$\begin{pmatrix} 0 & 0 & 0 \\ 0 & 0 & 0 \\ 0 & 0 & \varepsilon \end{pmatrix} \tag{7}$$

respectively. The associated energy changes are given, respectively, by

$$\Delta E(V_0) = V_0(C_{11} + C_{12})\varepsilon^2 \tag{8}$$

and

$$\Delta E(V_0) = \frac{1}{2}V_0 C_{33}\varepsilon^2. \tag{9}$$

The shear constant ($C_{11} - C_{12}$) was calculated by introducing a monoclinic distortion with the strain matrix

$$\begin{pmatrix} +\varepsilon & 0 & 0 \\ 0 & -\varepsilon & 0 \\ 0 & 0 & 0 \end{pmatrix}. \tag{10}$$

The associated energy change is given by

$$\Delta E(V_0) = V_0(C_{11} - C_{12})\varepsilon^2. \tag{11}$$

This distortion increases the $x$ axis and decreases the $y$ axis. The shear constant $C_{55}$ was calculated by introducing a triclinic distortion with the strain matrix

$$\begin{pmatrix} 0 & 0 & \varepsilon \\ 0 & 0 & 0 \\ \varepsilon & 0 & 0 \end{pmatrix} \tag{12}$$

and the associated energy change is given by

$$\Delta E(V_0) = 2V_0C_{55}\varepsilon^2. \tag{13}$$

We have used the highly accurate all-electron full-potential linear augmented plane wave (FLAPW) method [17] to calculate the total energies and magnetic properties of Fe, Co and Ni. The calculations are based on the first-principles density functional theory with the standard local density approximation (LDA) to the exchange-correlation potential [18]. The latest generalized gradient corrections (GGA) of Perdew-Burke-Ernzerhof [10] have been included in all the calculations. The muffin-tin radius used is 2.2 atomic units (a.u.). Fe $1s$, $2s$ and $2p$ are treated as core states, $3d$,$4s$ and $4p$ as band states and the shallow core states $3s$ and $3p$ are also treated as band states by using the so-called local orbitals [17]. For Co and Ni, $3s$ state is also treated as a core state. Inside the muffin-tin spheres, the wavefunctions, charge densities, and potential are expanded in terms of the spherical harmonics. The cut-off angular momentum ($L_{max}$) is 10 for the wave functions and 4 for charge densities (potentials). The Brillouin zone integration is carried out by using the improved tetrahedron method [19]. The number of the augmented plane waves included is about 90 per atom, i.e., $R_{mt}K_{max} = 9$ [17]. The numbers of the $k$-points in the irreducible Brillouin zone wedge (IBZW) for nonmagnetic and ferromagnetic bcc, fcc and hcp are, respectively, 104, 72, 120. The self-consistent cycles are terminated when the total energy converges to within 0.01 mRy/atom. In the shear constant calculations, the crystal is elastically deformed and may have a lower symmetry. Furthermore, the total energy change due to a shear strain is often very small (a few tenths of mRy/atom). Thus, more $k$-points in the IBZW are used. For example, when calculating hcp $C_{55}$, we used about 900 $k$-points. The self-consistent cycles are terminated when the total energy converges to within 0.002 mRy/atom.

## III. Total energy and lattice constants

### III-1. Iron

The calculated total energy as a function of volume per atom for bcc, fcc and hcp Fe is displayed in Fig. 1. Both the nonmagnetic and ferromagnetic states are considered. For the total energies of the hcp structure in Fig. 1, the theoretical $c/a$ ratios of 1.73 and 1.59 have been used for the ferromagnetic and nonmagnetic cases, respectively. The $c/a$ ratio was determined as follows. In each case, the $c/a$ ratio was initially fixed at the ideal value of 1.63 while the total energy was calculated for different volumes. The volume was then fixed at the minimal energy one while the total energy was calculated for different $c/a$ ratios to find the minimal energy $c/a$. This procedure was repeated till we found the change in the $c/a$ to be within 1 %. The theoretical $c/a$ ratio for the nonmagnetic phase is in good agreement with the previous GGA calculations [20, 21]. Each total energy vs volume per atom was fitted to the equation of state of Murnaghan [15] to obtain the theoretical lattice constant, bulk modulus and minimal total energy. The results are listed in Table I. Fig. 1 shows that the ferromagnetic bcc structure is the ground state for Fe, in agreement with the experiments and also with the previous GGA calculations [11]. The calculated bcc lattice constant $a$ is only 1 % smaller than the experimental value (Table I). The calculated bulk modulus $B$ is also in satisfactory agreement with experiments (Table I). Fig. 1 indicates that under pressure, ferromagnetic bcc Fe would first transform to nonmagnetic hcp structure. The theoretical transition pressure is estimated to be 121 kbar, be rather close to the value of 130 kbar determined experimentally [22]. Furthermore, the theoretical $c/a$ ratio of 1.59 is close to the experimental values in the pressure range of 150 $\sim$ 3000 kbar [22, 23]. In contrast, the LDA calculations [7, 8] predicted a wrong ground state (non-magnetic fcc), the ferromagnetic bcc lattice constant being 4 % too small and the bulk modulus of the ferromagnetic bcc structure being 50 % too large. In short, the present LDA-GGA calculations not only give a correct

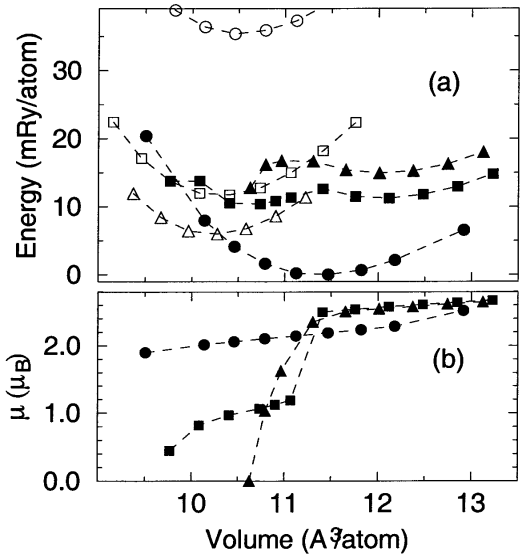


FIG. 1. (a) Total energy (relative to -2545.611 Ry/atom) of Fe as a function of volume per atom for bcc (circles), fcc (squares) and hcp (triangles). The curves are a polynomial fit to the total energies. Solid symbols denote the ferromagnetic states and open symbols, the nonmagnetic states. (b) Magnetic moment ($\mu$) of bcc, fcc and hcp Fe as a function of volume per atom.

TABLE I. The theoretical and experimental lattice constant ($a_0$), atomic volume ($V_0$),elastic constants, magnetic moment $m_s$ and total energy ($E_0$) of bcc, fcc and hcp Fe. Both nonmagnetic (NM) and ferromagnetic (FM) results are listed. The total energy of NM and FM hcp Fe is, respectively, -2545.6047 and -2545.5958 Ry/atom. The experimental values for the ferromagnetic bcc Fe (Exp[a]) [14] and for the nonmagnetic hcp Fe at 500 kbar (Exp[b]) [22] are also listed for comparison.

(a)

| bcc Fe | $a_0$ | $V_0$ | $B$ | $C'$ | $C_{11}$ | $C_{12}$ | $C_{44}$ | $m_s$ | $E_0$ |
|---|---|---|---|---|---|---|---|---|---|
| | Å | Å$^3$/atom | Mbar | Mbar | Mbar | Mbar | Mbar | $\mu_B$ | Ry/atom |
| FM | 2.84 | 11.40 | 1.86 | 0.69 | 2.79 | 1.40 | 0.99 | 2.17 | -2545.6107 |
| Exp[a] | 2.87 | 11.82 | 1.72 | 0.48 | 2.32 | 1.36 | 1.17 | 2.22 | |
| NM | 2.76 | 10.52 | 2.76 | -1.10 | 1.30 | 3.49 | 1.41 | | -2545.5754 |

(b)

| fcc Fe | $a_0$ | $V_0$ | $B$ | $C'$ | $C_{11}$ | $C_{12}$ | $C_{44}$ | $m_s$ | $E_0$ |
|---|---|---|---|---|---|---|---|---|---|
| | Å | Å $^3$/atom | Mbar | Mbar | Mbar | Mbar | Mbar | $\mu_B$ | Ry/atom |
| FM | 3.63 | 11.97 | 1.82 | -0.77 | 0.79 | 2.33 | 0.23 | 2.55 | -2545.5902 |
| NM | 3.45 | 10.30 | 3.17 | 1.25 | 4.84 | 2.34 | 2.87 | | -2545.5908 |

(c)

| hcp | $a_0$ | $c/a$ | $V_0$ | $B$ | $C_{11}$+$C_{12}$ | $C_{11}$-$C_{12}$ | $C_{11}$ | $C_{12}$ | $C_{13}$ | $C_{33}$ | $C_{55}$ | $m_s$ |
|---|---|---|---|---|---|---|---|---|---|---|---|---|
| Fe | Å | | Å$^3$/atom | Mbar | Mbar | Mbar | Mbar | Mbar | Mbar | Mbar | Mbar | $\mu_B$ |
| FM | 2.52 | 1.732 | 12.04 | 1.56 | 4.17 | -0.29 | 1.94 | 2.23 | 0.87 | 3.14 | -0.62 | 2.54 |
| NM | 2.46 | 1.586 | 10.23 | 2.97 | 7.27 | 3.85 | 5.56 | 1.71 | 1.43 | 6.47 | 2.48 | |
| Exp[b] | | | 8.89 | | 9.40 | 3.40 | 6.40 | 3.00 | 2.55 | 6.50 | 4.20 | |

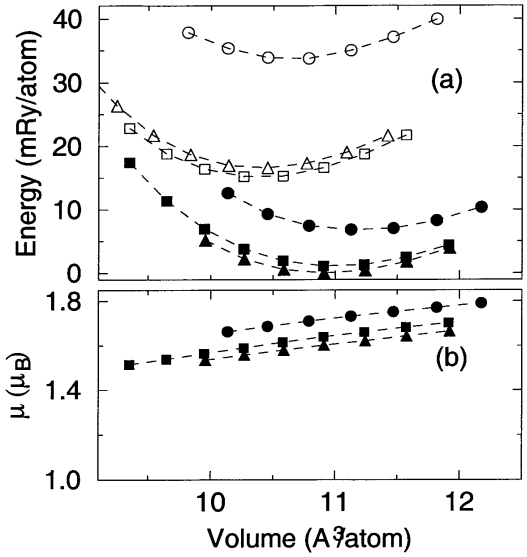


FIG. 2. (a) Total energy (relative to -2786.956 Ry/atom) of Co as a function of volume per atom for hcp (triangles), fcc (squares) and bcc (circles). The curves are a polynomial fit to the total energies. Solid symbols denote the ferromagnetic states and open symbols, the nonmagnetic states. (b) Magnetic moment ($\mu$) of hcp, fcc and bcc Co as a function of volume per atom.

ground state structure of Fe but also describe accurately the lattice constant and structural transformations under pressure.

The calculated spin magnetic moments for the ferromagnetic bcc, fcc and hcp are also shown in Fig. 1 as a function of volume per atom. Interestingly, the magnetic moments of both close-packed structures changes dramatically with volume when the volume is less than 11.5 Å$^3$/atom. For example, the magnetic moment of fcc phase clapses completely at 10.6 Å$^3$/atom whilst at 11.5 Å$^3$/atom it is as large as 2.5 $\mu_B$. In constrast, the magnetic moment of bcc Fe decreases monotonically and slowly as the volume is compressed. Nonetheless, these interesting behaviors of the magnetic moments of the close-packed structures of Fe have been elaborated already in several previous papers [24, 25]. Thus they will not be discussed further in this paper except that the calculated spin magnetic moment of the bcc phase agrees well with the experiments (Table I).

### III-2. Colbalt

The calculated total energy and spin magnetic moment as a function of volume per atom for hcp, fcc and bcc Co is displayed in Fig. 2. Both the nonmagnetic and ferromagnetic states are considered. For the total energies of the hcp structure in Fig. 2, the theoretical $c/a$ ratio of 1.62 has been used for both the ferromagnetic and nonmagnetic states. The theoretical lattice constant, bulk modulus and minimal total energy determined from these total energy vs volume curves are listed in Table II. Fig. 2 shows that the ferromagnetic hcp structure is the ground state for Co, in agreement with the experiments [14]. However, the total energy vs volume of ferromagnetic fcc Co lies immediately above the hcp phase, the energy difference between these two phases is only

TABLE II. The theoretical and experimental lattice constant ($a_0$), atomic volume ($V_0$), elastic constants, magnetic moment ($m_s$), total energy ($E_0$) of hcp, fcc and bcc Co. Both the nonmagnetic (NM) and ferromagnetic (FM) results are listed. The total energy of NM and FM hcp Co is, respectively, -2786.9397 and -2786.9563 Ry/atom. The experimental values for ferromagnetic hcp Co (Exp[a]) [14, 26] and ferromagnetic fcc Co (Exp[b]) [27] are also listed for comparison.

(a)

| hcp | $a_0$ | $c/a$ | $V_0$ | $B$ | $C_{11}$+$C_{12}$ | $C_{11}$-$C_{12}$ | $C_{11}$ | $C_{12}$ | $C_{13}$ | $C_{33}$ | $C_{55}$ | $m_s$ |
|---|---|---|---|---|---|---|---|---|---|---|---|---|
| Co | Å | | Å$^3$/atom | Mbar | Mbar | Mbar | Mbar | Mbar | Mbar | Mbar | Mbar | $\mu_B$ |
| FM | 2.50 | 1.62 | 10.92 | 2.21 | 5.41 | 1.65 | 3.53 | 1.88 | 1.16 | 4.43 | 0.63 | 1.60 |
| Exp[b] | 2.51 | 1.62 | 11.09 | 1.91 | 4.72 | 1.42 | 3.07 | 1.65 | 1.03 | 3.58 | 0.76 | 1.58 |
| NM | 2.45 | 1.62 | 10.41 | 2.62 | 6.30 | 4.54 | 5.42 | 0.88 | 2.51 | 1.68 | 1.29 | |

(b)

| fcc Co | $a_0$ | $V_0$ | $B$ | $C'$ | $C_{11}$ | $C_{12}$ | $C_{44}$ | $m_s$ | $E_0$ |
|---|---|---|---|---|---|---|---|---|---|
| | Å | Å$^3$/atom | Mbar | Mbar | Mbar | Mbar | Mbar | $\mu_B$ | Ry/atom |
| FM | 3.53 | 10.99 | 2.16 | 0.68 | 3.25 | 1.89 | 1.56 | 1.64 | -2786.0552 |
| Exp[a] | 3.55 | 11.14 | | | | | | 1.72 | |
| NM | 3.46 | 10.39 | 2.60 | 1.22 | 4.30 | 1.86 | 1.80 | | -2786.9411 |

(c)

| bcc Co | $a_0$ | $V_0$ | $B$ | $C'$ | $C_{11}$ | $C_{12}$ | $C_{44}$ | $m_s$ | $E_0$ |
|---|---|---|---|---|---|---|---|---|---|
| | Å | Å $^3$/atom | Mbar | Mbar | Mbar | Mbar | Mbar | $\mu_B$ | Ry/atom |
| FM | 2.82 | 11.18 | 2.09 | -0.24 | 1.93 | 2.41 | 1.31 | 1.73 | -2786.9395 |
| NM | 2.77 | 10.63 | 2.47 | -2.70 | -1.16 | 4.24 | 3.68 | | -2786.0225 |

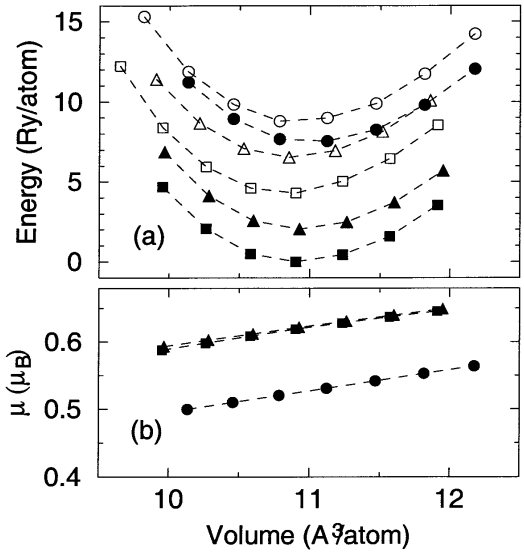


FIG. 3. (a) Total energy (relative to -3041.667 Ry/atom) of Ni as a function of volume per atom for fcc (squares), hcp (triangles), bcc (circles). The curves are a polynomial fit to the total energies. Solid symbols denote the ferromagnetic states and open symbols, the nonmagnetic states. (b) Magnetic moment ($\mu$) of fcc, hcp and bcc Ni as a function of volume per atom.

1 mRy/atom. Furthermore, all the calculated elastic constants are positive (see next section). This explains why the artificial fcc Co films can be grown up to 2000 Å [27]. The calculated hcp and fcc lattice constants differ from the corresponding experimental values only by less than 0.5 % (Table II). The calculated $B$ is however 15 % larger than the experimental value (Table I). Note that the theoretical bcc Co lattice constant (2.82 Å) is also close to that (2.83 Å) of the artificial Co bcc structure [2]. Unlike iron (Fig. 1), the total energy vs volume phase diagram (Fig. 2) is simple. All the magnetic curves lie below the nonmagnetic ones and show no kink or other anomalies. Furthermore, the calculated magnetic moments for the hcp, fcc and bcc show an expected behavior, i.e., the magnetic moment decreases monotonically with the volume. The bcc structure has a highest magnetic moment at all the volumes considered. The calculated spin magnetic moment at the minimal energy lattice constant for hcp Co is somewhat larger than the experimental one. For fcc Co the calculated and measured spin magnetic moments agree well (Table II).

### III-3. Nickel

The calculated total energy and spin magnetic moment as a function of volume per atom for fcc, hcp and bcc Ni is displayed in Fig. 3. Both the nonmagnetic and ferromagnetic states are considered. For the total energies of the hcp structure in Fig. 3, the theoretical $c/a$ ratio of 1.65 has been used for the ferromagnetic and nonmagnetic phases. This $c/a$ value is in good agreement with a very recent calculation [21]. The theoretical lattice constant, bulk modulus and minimal total energy determined from these total energy vs volume curves are listed in Table III.

TABLE III. The theoretical and experimental lattice constant ($a_0$), atomic volume ($V_0$), elastic constants, magnetic moment ($m_s$), and total energy ($E_0$) of bcc, fcc and hcp Ni. Both the nonmagnetic (NM) and ferromagnetic (FM) results are listed. The total energy of NM and FM hcp Ni is, respectively, -3041.6602 and -3041.6647 Ry/atom. The experimental values for the ferromagnetic fcc Ni (Exp) [14] are also listed for comparison.

(a)

| fcc Ni | $a_0$ | $V_0$ | $B$ | $C'$ | $C_{11}$ | $C_{12}$ | $C_{44}$ | $m_s$ | $E_0$ |
|---|---|---|---|---|---|---|---|---|---|
| | Å | Å$^3$/atom | Mbar | Mbar | Mbar | Mbar | Mbar | $\mu_B$ | Ry/atom |
| FM | 3.52 | 10.92 | 1.99 | 0.66 | 2.87 | 1.55 | 1.50 | 0.62 | -3041.6667 |
| Exp | 3.52 | 11.09 | 1.86 | 0.54 | 2.48 | 1.55 | 1.24 | 0.61 | |
| NM | 3.51 | 10.83 | 2.07 | 0.83 | 3.23 | 1.62 | 0.39 | | -3041.6624 |

(b)

| hcp | $a_0$ | $c/a$ | $V_0$ | $B$ | $C_{11}$+$C_{12}$ | $C_{11}$-$C_{12}$ | $C_{11}$ | $C_{12}$ | $C_{13}$ | $C_{33}$ | $C_{55}$ | $m_s$ |
|---|---|---|---|---|---|---|---|---|---|---|---|---|
| Ni | Å | | Å$^3$/atom | Mbar | Mbar | Mbar | Mbar | Mbar | Mbar | Mbar | Mbar | $\mu_B$ |
| FM | 2.48 | 1.645 | 10.93 | 2.00 | 4.98 | 2.89 | 3.94 | 1.05 | 1.30 | 3.76 | 1.05 | 0.62 |
| NM | 2.47 | 1.649 | 10.87 | 2.22 | 4.56 | 1.79 | 3.18 | 1.39 | 2.28 | 1.76 | 1.57 | |

(c)

| bcc NI | $a_0$ | $V_0$ | $B$ | $C'$ | $C_{11}$ | $C_{12}$ | $C_{44}$ | $m_s$ | $E_0$ |
|---|---|---|---|---|---|---|---|---|---|
| | Å | Å $^3$/atom | Mbar | Mbar | Mbar | Mbar | Mbar | $\mu_B$ | Ry/atom |
| FM | 2.80 | 11.02 | 1.96 | -0.33 | 1.57 | 2.23 | 1.56 | 0.53 | -3041.6592 |
| NM | 2.80 | 10.93 | 2.04 | -0.96 | 0.84 | 2.76 | 3.95 | | -3041.6579 |

Fig. 3 shows that the ferromagnetic fcc structure is the ground state for Ni, in agreement with the experiments [14]. Furthermore, the calculated fcc lattice constant $a$ is only 0.5 % smaller than the experimental value (Table III). The calculated $B$ is 7 % larger than the experimental value (Table III). Note that artificial hcp $Ni_{1-x}Fe_x$ ($0 < x < 20\%$) films were recently made [28]. The lattice parameters $a$ of 2.50 Å and $c$ of 4.07 Å are close to the theoretical values calculated here

(Table III). Unlike iron (Fig. 1), the total energy vs volume phase diagram (Fig. 2) is simple. All the magnetic curves lie below the associated nonmagnetic ones, respectively and show no kink or other anomalies. Furthermore, the calculated magnetic moments for the hcp, fcc and bcc show an expected behavior, i.e., the magnetic moment decreases monotonically with the volume. The calculated and measured spin magnetic moments agree very well. Unlike bcc Co, the bcc Ni has a smallest magnetic moment among the three structures. Furthermore, the magnetization energy of the bcc structure is small and the energy of the ferromagnetic bcc is still above that of the nonmagnetic fcc and hcp phases (Fig. 3).

## IV. Elastic constants

### IV-1. Irons

The theoretical shear constants of bcc, fcc and hcp Fe in both ferromagnetic and nonmagnetic states calculated as described in Sec. II, are listed in Table I. All the elastic constants for each of these phases derived from the calculated shear constants and bulk modulus, are listed in table 1. Table I shows that for the ferromagnetic bcc structure, the calculated and measured elastic constants agree within 20 %. This level of the agreement is considered to be satisfactory because, unlike the calculations of lattice constants and bulk modulus, the calculated elastic constants are rather sensitive to the numerical uncertainties and thus much more demanding. Interestingly, some experimental elastic constants of nonmagnetic hcp Fe measured at 500 kbar [22] (also listed in Table I) are close to the calculated values for the same structure.

From Fig. 1, all the six phases appear to be either a stable or metastable phase. As mentioned in Sec. 1, this is not necessarily the case. Table I shows that nonmagnetic bcc, ferromagnetic fcc and hcp Fe are not a metastable state since they are unstable against one shear deformation or another.

### IV-2. Colbalt

The theoretical shear constants of hcp, fcc and bcc Co in both ferromagnetic and nonmagnetic states calculated as described in Sec. II, are listed in Table II. All the elastic constants for each of these phases derived from the calculated shear constants and bulk modulus, are listed in Table II. Table II shows that for the ferromagnetic hcp structure, the calculated and measured elastic constants agree within up to 25 %. This level of the agreement is again considered to be rather satisfactory because of the reasons mentioned in the previous subsection. Unlike iron, only nonmagnetic and ferromagnetic bcc phases of Co are not a metastable state since they have negative shear constants (Table II). Furthermore, $C_{11}$ of the nonmagnetic bcc structure is also negative due to the large negative value of the shear constant $C'$.

### IV-3. Nickel

The theoretical shear constants of fcc, hcp and bcc Ni in both ferromagnetic and nonmagnetic states calculated as described in Sec. II, are listed in Table III. All the elastic constants for each of these phases derived from the calculated shear constants and bulk modulus, are listed in Table III. Table III shows that for the ferromagnetic fcc structure, the calculated and measured elastic constants agree within up to 20 %. This level of the agreement is considered to be satisfactory

because of the reasons mentioned before. Unlike iron but like colbalt, only nonmagnetic and ferromagnetic bcc phases of Co are not a metastable state since they have negative shear constants. Unlike bcc Co, $C_{11}$ of the nonmagnetic bcc Ni is positive.

## V. Discussion and summary

Remarkably, Tables I-III and Figures 1-3 show that the occurrence of magnetism in a solid not only increases its lattice constant and reduces its bulk modulus (i.e., makes the solid softer) but also affects its structural stability. These magnetic effects are particularly pronounced in iron perhaps because iron has a largest spin moment among the materials studied here. For example, the existence of the ferromagnetism increases the bcc Fe lattice constant by 4 % and reduces the bulk modulus by 45 % (Table I). Furthermore, nonmagnetic bcc Fe has the highest total energy among the phases considered (Fig. 1) and is elastically unstable (i.e., $C'$ is negative) (Table I). Ferromagnetism makes the bcc structure to become the ground state for iron and also elastically stable. It appears to be a rule of thumb that magnetism in a solid generally increases its lattice constant and reduces its bulk modulus (see, e.g., Tables I-III ). However, this is no general rule as how the magnetism would affect the phase stability and the total energy. For example, in contrast to the bcc Fe structure, the occurrence of the ferromagnetism destabilizes the fcc and hcp Fe structures which have certain negative elastic constants (Table I). The total energy of the nonmagnetic hcp Fe is lower than that of the ferromagnetic hcp Fe (Fig. 1).

Summarizing, we have carried out systematic LDA-GGA calculations of lattice constants, elastic constants and magnetic moments of Fe, Co and Ni in their three most common structures (i.e., bcc, fcc and hcp structures). We find that the GGA of Perdew, Burke and Ernzerhof [10] removes most of the errors found in the previous LDA calculations (e.g., [7, 8]). Notably, the LDA-GGA predicts a correct ground state structure for iron and a pressure-induced transformation from the ferromagnetic bcc to the nonmagnetic hcp structure with a transition pressure being close to the experimental value. Furthermore, the calculated lattice constants for all the three elements are in very good agreement with experiments. It is thus concluded that the LDA-GGA describes well the total energy vs structure phase diagram of the $3d$ transition metals. Currently, there is considerable interest in growing and studying the physical properties of artificial $3d$ magnetic thin films and superlattices. The LDA-GGA calculations would therefore help to gain insight into the phase stability, magnetism and other novel properties of these artificial made structures, and to provide some guidance to grow new metastable thin films and superlattices. In this context, the calculation of the minimal energy lattice constants and also elastic constants would be particularly interesting since a metastable structure is usually grown on a substrate with a similar lattice constant. We find that magnetism has pronounced effects on the lattice constant, the phase stability and also the ordering of the total energies of various structures.

The authors acknowledge support from the National Science Council of ROC (NSC 88-2112-M002-0043, NSC 89-2112-M002-0025).

## References

[ 1 ] W. Keune *et al*., J. Appl. Phys. **48**, 2976 (1977).

[ 2 ] G. A. Prinz, Phys. Rev. Lett. **54**, 1051 (1985).

[ 3 ] B. Heinrich *et al*., J. Vac. Sci. Technol. **A64**, 1376 (1986).
[ 4 ] P. Hohenberg and W. Kohn, Phys. Rev. **B136**, 864 (1964); W. Kohn and L.J. Sham, Phys. Rev. **A140**, 1133 (1965).
[ 5 ] R. O. Jones and O. Gunnarsson, Rev. Mod. Phys. **61**, 689 (1989).
[ 6 ] A. T. Paxton, M. Methfessel and H. M. Polatoglou, Phys. Rev. **B41**, 8127 (1990).
[ 7 ] C. S. Wang, B. M. Klein and H. Krakauer, Phys. Rev. Lett. **16**, 1852 (1985).
[ 8 ] G. Y. Guo *et al*., Solid State Comm. **79**, 121 (1991).
[ 9 ] V. L. Sliwko *et al*., J. Phys.: Condens. Matter **8**, 799 (1996).
[10] J. P. Perdew, S. Burke and M. Ernzerhof, Phys. Rev. Lett. **77**, (1996) 3865.
[11] D. J. Singh, W. E. Pickett and H. Krakauer, Phys. Rev. **B43**, 11628 (1991).
[12] A. T. Paxton, M. Methfessel and H. M. Polatoglou, Phys. Rev. **B41**, 8127 (1990).
[13] A. Y. Liu and D. J. Singh, Phys. Rev. **B47**, 8515 (1993).
[14] C. Kittel, *Introduction to Solid State Physics*, 7th ed. (Wiley, New York, 1996).
[15] F. D. Murnaghan, Proc. Nat. Acad. Sci. U.S.A. **3**, 244 (1944).
[16] L. Fast *et al*., Phys. Rev. **B51**, 17431 (1995).
[17] P. Blaha, K. Schwarz, and J. Luitz, WIEN97, Vienna University of Technology 1997. (Improved and updated Unix version of the original copyrighted WIEN-code, which was published by P. Blaha, K. Schwarz, P. Sorantin, and S.B. Trickey, in Comput. Phys. Commun. 59, 399 1990).
[18] D. M. Ceperley and B. J. Alder, Phys. Rev. Lett. **45**, 566 (1980).
[19] P. E. Blöchl, O. Jepsen and O. K. Andersen, Phys. Rev. **B49**, 16223 (1994).
[20] P. Söderlind, J. A. Moriarty, J. M. Wills, Phys. Rev. **B53**, 14063 (1996).
[21] J. X. Zheng-Johansson, O. Eriksson and B. Johansson, Phys. Rev. **B59**, 6131 (1999).
[22] A. P. Jephcoat, H. K. Mao, and P. M. Bell, J. Geophys. Res. **91**, 4677 (1986).
[23] H. K. Mao *et al*., J. Geophys. Res. **95**, 21737 (1990).
[24] V. L. Moruzzi *et al*., Phys. Rev. **B34**, 1784 (1986).
[25] P. M. Marcus, V. L. Moruzzi, S.-L. Qiu, Phys. Rev. **B60**, 369 (1999).
[26] H. J. McSkimin, J. Appl. Phys. **26**, 406 (1955).
[27] G. Harp *et al*., Phys. Rev. **B48**, 17538 (1993).
[28] J.C.A. Huang *et al*., Phys. Rev. **57**, 11517 (1998).